Active Authority Enhancement of Piezoelectric Actuator Design via Mechanical Resonance and Electrical Tailoring

J.-S. Kim*, K. W. Wang†, and E. C. Smith‡
The Pennsylvania State University, University Park, PA 16802

Abstract

In this research, a new approach is proposed to enhance the authority of piezoelectric actuators without the trade off between force and stroke. Through mechanical tailoring, the resonance frequencies of the actuator system can be tuned to the required actuation frequencies. This obviously will increase the authority (both stroke and force) of the actuator. However, resonant actuators could be hard to control and non-robust, due to its narrow operating bandwidth. This issue can be resolved through electric circuit tailoring. With the aid of a network of inductance, resistance, and negative capacitance, the actuation resonance peak can be significantly broadened and flattened. In this case, one can achieve a high authority actuator without the negative effects of resonance problems. The electrical networks can also achieve a fail-safe system due to its passive shunting characteristic. The proposed concept is evaluated and compared on three types of PZT actuators (benders, stacks and tubes) for trailing edge flap control of rotorcraft blades. Promising results are demonstrated, showing that the treatment can indeed create a high authority and robust actuator that satisfies the performance requirements of the example system.

1 Introduction

Active actuator technologies utilizing piezoelectric materials have been given considerable attention in recent years for various engineering applications. Such actuators are appealing because electrical input energy is directly converted to mechanical output energy, and they are able to produce high actuation bandwidth, large forces, and high energy densities. It has been shown that improvement in helicopter vibration reduction may be feasible through utilizing active control technology via PZT actuators. Numerous approaches have been investigated to develop actuation mechanisms exploiting the characteristics of piezoelectric ceramic materials. Among them, one of the very promising concepts for helicopter rotor control is the active trailing edge flap [1,2,3]. Such an actuation system can be used with multi-functional roles to suppress vibration and noise, increase aeromechanical stability, and decrease blade loads.

While current piezoelectric materials-based actuators have shown good potential in actuating trailing edge flaps, but can only provide a limited stroke, about 2~4 degrees. This limitation can be critical in case where large trailing edge flap deflections are required. The efforts to improve the PZT actuator performance have been made by researchers in developing actuation mechanisms of various types [4-9]. In general, these devices require a trade off between force and stroke and are still limited in their performance.

The goal of this research is to develop a new method for active authority enhancement of piezoelectric actuation systems, without the tradeoff between stroke and force. The trailing edge flap is used as a test bed for illustrating the concept. The approach can be classified into two stages as outlined in the following paragraphs.

First, a selected resonant frequency of the actuation system (composed of the piezoelectric actuator, the trailing edge flap and the amplification mechanism, and under the effect of unsteady aerodynamic loads) is tuned to the desired operating frequency through mechanical tailoring. It is well known that, for harmonic control devices such as the trailing edge flaps, if one can tune the natural frequencies of the actuator system to the actuation frequencies, the authority (both stroke and force) can be greatly increased due to the mechanical resonance effect. In this case, one can develop much lighter and smaller actuators to activate multiple and smaller trailing edge flaps, each aiming at different operating frequencies of 3, 4, and 5/rev of the main rotor. While such a concept is indeed attractive, resonant actuators could be very difficult to control and non-robust, due to its narrow operating bandwidth. This is a critical bottleneck for realizing resonant actuation system in practical applications.

---

* Graduate Research Assistant, Presenting author.
† William E. Diefenderfer Chaired Professor in Mechanical Engineering, Corresponding author.
(E-mail: kwwang@psu.edu, Tel: (814)865-2183, Fax: (814)863-7222)
‡ Associate Professor in Aerospace Engineering
Presented at the Fifth International Conference on Intelligent Materials, June 14 - 17, 2003, University Park, PA

Report Documentation Page

Form Approved
OMB No. 0704-0188

1. REPORT DATE	2. REPORT TYPE	3. DATES COVERED
00 JUN 2003	**N/A**	**-**

4. TITLE AND SUBTITLE	5a. CONTRACT NUMBER
Active Authority Enhancement of Piezoelectric Actuator Design via Mechanical Resonance and Electrical Tailoring	5b. GRANT NUMBER
	5c. PROGRAM ELEMENT NUMBER
6. AUTHOR(S)	5d. PROJECT NUMBER
	5e. TASK NUMBER
	5f. WORK UNIT NUMBER
7. PERFORMING ORGANIZATION NAME(S) AND ADDRESS(ES) **The Pennsylvania State University, University Park, PA 16802**	8. PERFORMING ORGANIZATION REPORT NUMBER
9. SPONSORING/MONITORING AGENCY NAME(S) AND ADDRESS(ES)	10. SPONSOR/MONITOR'S ACRONYM(S)
	11. SPONSOR/MONITOR'S REPORT NUMBER(S)

12. DISTRIBUTION/AVAILABILITY STATEMENT
Approved for public release, distribution unlimited

13. SUPPLEMENTARY NOTES
See also ADM001697, ARO-44924.1-EG-CF, International Conference on Intelligent Materials (5th)(Smart Systems & Nanotechnology)., The original document contains color images.

14. ABSTRACT

15. SUBJECT TERMS

16. SECURITY CLASSIFICATION OF:			17. LIMITATION OF ABSTRACT	18. NUMBER OF PAGES	19a. NAME OF RESPONSIBLE PERSON
a. REPORT	b. ABSTRACT	c. THIS PAGE			
unclassified	**unclassified**	**unclassified**	**UU**	**12**	

To resolve this issue, the second step of this design process is to use electric circuitry tailoring to broaden and flatten the frequency response resonant peak, so that one can achieve a high authority actuation system with sufficient bandwidth and robustness. In the last decade, piezoelectric materials with electrical networks have been utilized to create shunt damping for structural vibration suppression. It was also recognized that such networks not only can be used for passive damping, they can also be designed to amplify the actuator active authority around the tuned circuit frequency [10-12]. Several researchers have proposed the "negative capacitance" concept to enhance the networks' multiple mode and broadband capabilities [13,14]. The integration of the passive and active approach, often referred to as an active-passive hybrid piezoelectric network, has shown to achieve promising results in vibration control [15]. The electric network tailoring idea proposed in this paper is built upon these previous investigations, but with completely different design philosophy and criterion.

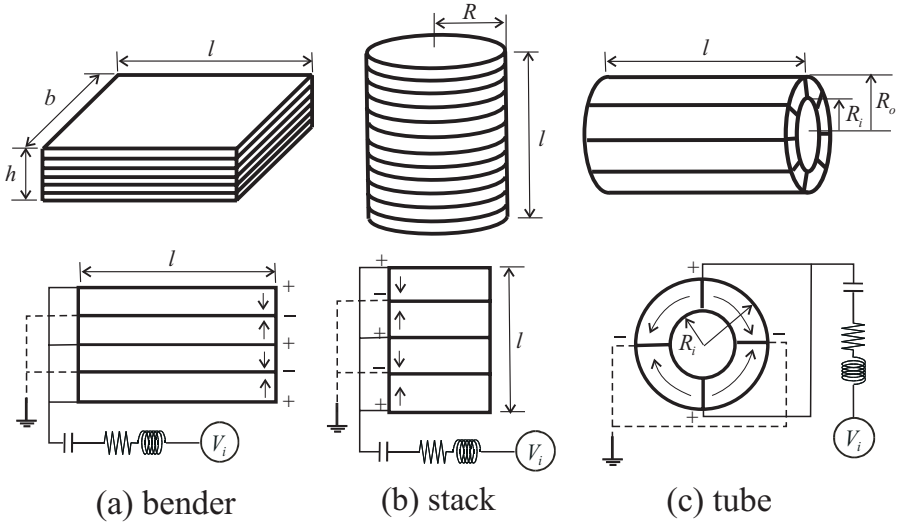

Figure 1: Piezoelectric bender, stacks, and tube actuators with electric networks

To demonstrate the proposed actuation mechanism, three types of PZT actuators, namely the bender, stack and tube, are selected for study in this investigation (Figure 1). Fully coupled PZT/trailing edge flap/circuit system model equations are derived for each of the actuators. The proposed method is applied to all three actuation systems and their performances are analyzed and compared.

2 Modeling of Piezoelectric Actuators

One general form of the constitutive equations of a linear piezoelectric material is shown below [16] ,

$$\begin{aligned} T_i &= c_{ij}^D S_j - h_{ik} D_k \\ E_l &= -h_{lj} S_j + \beta_{lk}^S D_k \end{aligned} \qquad (i, j = 1,2,...,6),\ (k,l = 1,2,3), \tag{1}$$

where T_i, S_j, D_k, and E_k represent the stress, strain, electrical displacement (charge/area) and electrical field (voltage/length) of the piezoelectric material, respectively. $C_{ij}^{\ D}$ are the elastic constants, h_{ik} are the piezoelectric constants, and $\beta_{lk}^{\ S}$ are the impermittivity components (dielectric constants). Superscript 'D' and 'S' indicate the parameter values at constant electric displacement and strain, respectively. For bender, stack and tube types of piezoelectric actuators, their corresponding specific constitutive equations are presented in Table 1.

The system equations of motion are derived using Hamilton's principle and discretized by applying the assumed mode method. In this study, we will focus on a single mode model of the actuators. Thus, the PZT actuator displacement is assumed to be

$$u(x,t) = \phi(x) q(t) \tag{2}$$

where $\phi(x)$ is the first eigenfunction of the actuator without electrical networks, and $q(t)$ is the generalized mechanical displacement. The PZT bender, stack, and tube actuators are modeled by clamped-free beam, cylinder, and hollow cylinder, respectively (see Figure 1).

Table 1: Constitutive equations for each type of actuator

Actuator	Bender	Stack	Tube
Piezoelectric constitutive equations	$T_1 = c_{11}^D S_1 - h_{13} D_3$ $E_3 = -h_{31} S_1 + \beta_{33}^S D_3$	$T_3 = c_{33}^D S_3 - h_{33} D_3$ $E_3 = -h_{33} S_3 + \beta_{33}^S D_3$	$T_5 = c_{55}^D S_5 - h_{51} D_1$ $E_1 = -h_{15} S_5 + \beta_{11}^S D_1$

The actuation mechanisms of the three actuator types are different. First, for the bender actuator, it is cantilevered and equal but opposite electric field is applied to the PZT sheets on opposite sides of the mid-plane. This causes a pure bending of the PZT beam and the resulting tip displacement provides the stroke for the trailing edge flap. The stack actuator consists of many thin layers of PZT sheets alternatively connected to positive and negative terminals of a voltage source. When an electrical voltage is applied, each PZT material layer expands and produces a net output displacement. Last, the tube actuator, which uses the shear deformation of PZT material, is assembled with PZT ceramic segments of alternating poling signs, and then the accumulation of shear strain around the circumference produces the angle of twist. Both bender and stack actuators are poled in the thickness direction, while tube actuator is poled in the circumference direction. Therefore, the electrical field to be applied is E_3 for bender and stack, and E_1 for tube.

The bender actuator is modeled by the classical Euler-Bernoulli's beam theory. The stack and tube actuators are modeled as simple rod and torsion bar, respectively. The bonding layer between PZT sheets or segments is neglected. For a bender actuator, the first eigenfunction is given by,

$$\phi(x) = \sin(\tfrac{\beta}{l}x) - \sinh(\tfrac{\beta}{l}x) - \alpha\{\cos(\tfrac{\beta}{l}x) - \cosh(\tfrac{\beta}{l}x)\}, \tag{3}$$

where α and β denote the coefficients of clamped beam eigenfunctions [19], l indicates the length of the beam, and x is the distance along span of the beam.

For stack and tube actuators,

$$\phi(x) = \sin(\frac{\pi}{2l}x). \tag{4}$$

For each actuator, the equations of motions can be written as follows:

$$\begin{aligned} &M_P\ddot{q} + C_P\dot{q} + K_P q + k_1 Q = F \\ &V_a = k_2 + k_1 q \end{aligned} \tag{5}$$

where M_p, C_p and K_p are the mass, damping, and open-circuit stiffness terms of the actuator, and Q is the charge on the piezoelectric material. k_1 represents the coupling between the mechanical and electrical variables, F is the excitation force, V_a is the voltage across the actuator, which is used to integrate the circuit equation into the actuator model, k_2 represents the inverse of the capacitance of the piezoelectric actuators at constant strain ($1/C_p^S$). Analytical expressions of the stiffness, mass, coupling and capacitance terms are listed and compared in Table 2, where n is the number of PZT sheets or segments, t is the thickness of a sheet, and the dimensions of PZT actuators (l,b,R,R_o,R_i) are shown in Fig. 1.

Table 2: Stiffness, mass, coupling and capacitance of piezoelectric actuators

Actuator	Bender	Stack	Tube
Stiffness, K_P	$\int_0^l (\frac{1}{12}bh^3) c_{11}^D \phi_{,xx}^2 dx$	$\int_0^l (\pi R^2) c_{33}^D \phi_{,x}^2 dx$	$\int_0^l \frac{\pi}{2}(R_o^4 - R_i^4) c_{55}^D \phi_{,x}^2 dx$
Mass, M_P	$\int_0^l \rho(bh)\phi^2 dx$	$\int_0^l \rho(\pi R^2)\phi^2 dx$	$\int_0^l \rho \frac{\pi}{2}(R_o^4 - R_i^4)\phi^2 dx$
Coupling, k_1	$\frac{nt^2}{4l}\int_0^l h_{13}\phi_{,xx} dx$	$-\frac{1}{n}\int_0^l h_{33}\phi_{,x} dx$	$-\frac{2\pi}{3nl}\frac{(R_o^3 - R_i^3)}{(R_o - R_i)}\int_0^l h_{15}\phi_{,x} dx$
Capacitance, C_P^S	$\frac{nlb}{\beta_{33}^S t}$	$\frac{n(\pi R^2)}{\beta_{33}^S t}$	$\frac{n^2 l(R_o - R_i)}{\pi\beta_{11}^S(R_o + R_i)}$

3 Aerodynamic and inertial loads at trailing edge flap hinge

The aerodynamic model for trailing edge flap used in this study is based on the incompressible theory by Theodorsen [17]. The total hinge moment is comprised of the aerodynamic, inertial and centrifugal propeller moments due to the rotation of blade (see Figure 2). Assuming that the trailing edge flap deflection angles are small, the inertial and propeller moments can be expressed as:

$$h_I = I_\delta \ddot{\delta} \tag{6}$$

$$h_{CF} = M_f \Omega^2 d\ x_{xg}\ \sin(\delta) \approx M_f \Omega^2 d\ x_{xg} \delta \tag{7}$$

where δ is a trailing flap deflection angle, and Ω is the rotation speed of blade. I_δ, M_f, d and x_{cg} are the flap mass moment of inertia, the mass of flap, the distance of flap center of mass from elastic axis of blade and the distance from its hinge axis, respectively.

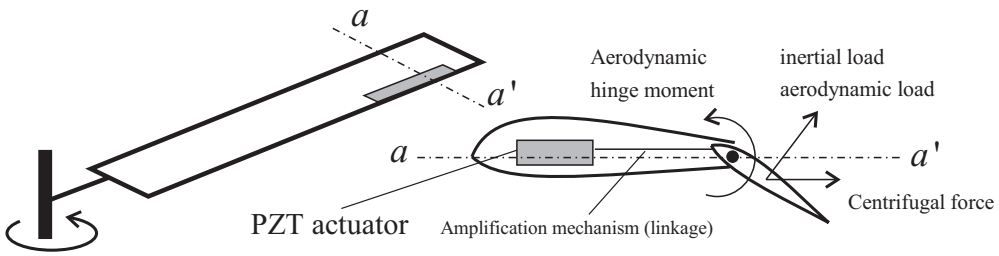

Figure 2: Moments and loads acting on trailing edge flap

The aerodynamic contribution due to trailing edge flap can be obtained from incompressible aerodynamic model based on Theodorsen's theory. The hinge moment coefficients in terms of flap deflection angle δ is given by

$$C_{H\delta} = -\frac{1}{2\pi} T_{12} T_{10} C(k) + \frac{1}{2\pi}(T_4 T_{10} - T_5) \tag{8}$$

$$C_{H\dot{\delta}} = -\frac{1}{4\pi U_\infty} T_{12} T_{11} b C(k) + \frac{1}{4\pi U_\infty} T_4 T_{11} b \tag{9}$$

$$C_{H\ddot{\delta}} = \frac{1}{2\pi U_\infty^2} T_3 b^2 \tag{10}$$

where coefficients T are geometric parameters defined by Theodorsen, U_∞ and b are the relative wind velocity at the radial location of flap and one half of the flap chord length, respectively. The Theodorsen lift deficiency function $C(k)$ is a complex coefficient that can be expressed in terms of Bessel functions. More detail expressions can be found in Ref. [17]. Once all the coefficients are found, aerodynamic and inertial contributions F_A can be expressed in terms of the trailing edge flap deflection angle δ:

$$F_A = M_A \ddot{\delta} + C_A \dot{\delta} + K_A \delta \tag{11}$$

in which,

$$M_A = \frac{1}{2} C_{H\ddot{\delta}} \rho_{air} U_\infty^2 c^2 L_f + h_I \tag{12}$$

$$C_A = \frac{1}{2} C_{H\dot{\delta}} \rho_{air} U_\infty^2 c^2 L_f \tag{13}$$

$$K_A = \frac{1}{2} C_{H\delta} \rho_{air} U_\infty^2 c^2 L_f + h_{CF} \tag{14}$$

where c and L_f are the chord length and span of trailing edge flap, respectively. Subscript 'A' indicates the trailing edge flap contribution.

4 Coupled Actuator/Flap/Circuit System

In this section, the coupled actuator/flap/circuit equations are derived to describe the integrated actuation system. For the single-frequency electric network (see Figure 3), a series R-L-C circuit is used and the resulting piezoelectric network equation can be written as

$$L\ddot{Q} + R\dot{Q} + \hat{k}_2 Q + k_1 q = V_C, \quad \frac{1}{\hat{k}_2} = C_P^E = \frac{C_n C_P^S}{C_P^S + C_n} \tag{15}$$

where L is the shunt inductance, R is the shunt resistance, and V_C represents the control voltage. C_P^E and C_n are the effective capacitance and negative capacitance, respectively. Here, the negative capacitance can be achieved using an operational amplifier to form a negative impedance converter circuit [18].

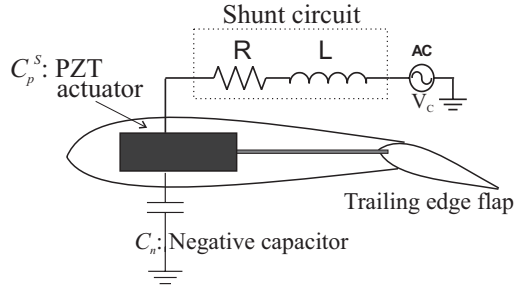

Figure 3: Schematic of PZT actuator with shunt circuit and negative capacitor.

In order to integrate the PZT actuator and the flap system, the trailing edge flap deflection angle, δ, should be expressed in terms of the actuator stroke, q. This relation can be interpreted as the amplification mechanism, i.e., the linkage from the PZT tube actuator to the flap device. The design of this linkage is not a trivial issue, which is beyond the scope of present study. Thus, the simple fulcrum type of amplification mechanism is used to illustrate the concept in this paper. It is assumed that the relation between δ and q can be expressed in the form

$$\delta = A_M q \,. \tag{16}$$

Note that this relationship, A_M, plays a role of unit conversion. For instance, the trailing edge flap deflection δ is transformed to the generalized displacement q of the PZT actuator. On the other hand, using the same relationship, the hinge moments are transformed to forces or moments, depending on the actuator types. For example, in case of the tube actuator, the hinge moment is transformed into torque.

Substituting Eq. (16) into Eq. (11) and combining Eq. (5) and Eq. (15) yield

$$\begin{aligned} M\ddot{q} + C\dot{q} + Kq + k_1 Q &= \hat{F} \\ L\ddot{Q} + R\dot{Q} + \hat{k}_2 Q + k_1 q &= V_C \end{aligned} \tag{17}$$

where

$$\begin{aligned} M &= M_P + M_A A_M \\ C &= C_P + C_A A_M \\ K &= K_P + K_A A_M \end{aligned} \tag{18}$$

The transfer functions between structural response and inputs (external force and control voltage) are given by

$$G_{qF}(\omega) = \frac{q(\omega)}{\hat{F}(\omega)} = \frac{\hat{k}_2 - \omega^2 L + i\omega R}{(\hat{k}_2 - \omega^2 L + i\omega R)(K - \omega^2 M + i\omega C) - k_1^2} \tag{19a}$$

and

$$G_{qV}(\omega)=\frac{q(\omega)}{V_C(\omega)}=\frac{-k_1}{(\hat{k}_2-\omega^2L+i\omega R)(K-\omega^2M+i\omega C)-k_1^2} \tag{19b}$$

where the frequency response, $q(\omega)$, represents the actuator stroke (e.g., tip deflection of the bender, tip twist angle of the tube actuator, and tip axial displacement of the stack). The adding of an inductor forms a resonant circuit, a resistor plays the role of damping and a negative capacitance tends to reduce the electrical stiffness so that the voltage driving response increases over the entire frequency range and broadens around resonance peak.

To investigate the coupled system characteristics, Eq. (19) is nondimensionalized as:

$$\overline{G}_{qF}=\frac{G_{qF}}{G_{qF}^{ST}}=\frac{(\delta^2-\varpi^2)+ir\delta^2\varpi}{(1-\varpi^2+\xi^2\eta^2+i2\zeta\varpi)(\delta^2-\varpi^2+ir\delta^2\varpi)-\delta^2\xi^2\eta^2} \tag{20a}$$

and

$$\overline{G}_{qV}=\frac{G_{qV}}{G_{qV}^{ST}}=\frac{\delta^2}{(1-\varpi^2+\xi^2\eta^2+i2\zeta\varpi)(\delta^2-\varpi^2+ir\delta^2\varpi)-\delta^2\xi^2\eta^2} \tag{20b}$$

in which,

$$\begin{gathered}\omega_c=\sqrt{\frac{K-k_1^2/\hat{k}_2}{M}},\ \omega_m=\sqrt{\frac{K}{M}},\ \omega_e=\sqrt{\frac{\hat{k}_2}{L}},\ \zeta=\frac{C}{2M\omega_c},\ \xi=\frac{k_1}{\sqrt{K\hat{k}_2}}\\ \eta=\frac{\omega_m}{\omega_c},\ \varpi=\frac{\omega}{\omega_c},\ \delta=\frac{\omega_e}{\omega_c},\ r=\frac{R}{\hat{k}_2}\omega_c\\ G_{qF}^{ST}=\frac{\eta^2}{\omega_m^2M},\ G_{qV}^{ST}=\frac{\xi^2\eta^2}{k_1}\end{gathered} \tag{21}$$

where r and δ represent the resistance and inductance tuning ratios, ξ denotes the generalized electro-mechanical coupling coefficient, and η is the frequency ratio between electro-mechanical de-coupled and coupled systems. Superscript '*ST*' indicates the static system. Subscript '*c*' and '*m*' denote the electro-mechanical coupled and de-coupled systems, respectively, and subscript '*e*' represents the electrical system.

In this paper, Eqs. (19a) and (20a) are referred to as the *passive damping* responses, since they represent the response of the actuation system under external loading, but in a passive mode without active action. On the other hand, Eqs. (19b) and (20b) are referred to as the *voltage driving* responses representing the stroke of the actuation system under given electric voltage input.

5 Mechanical and Electrical Tailoring

5.1 Mechanical tailoring

In the present study, structural resonance of the actuation system is utilized to increase the active authority. The stiffness and/or the mass of the coupled system could be adjusted to tune the resonant frequency of the actuation system to around the desired operating frequency.

It is assumed that the stiffness and mass of the PZT actuators is fixed, and the modal stiffness and mass of the trailing edge flap and the amplification mechanism could be adjusted. Tuning the mass will be more effective than tuning the stiffness because the mass of the coupled system mostly comes from the aerodynamic contribution (the flap mass moment of inertia in Eq. (6)). There are two ways to adjust the mass term of the aerodynamic loads. One is to add concentrated mass to the trailing edge flap. This is the simplest method to adjust the mass term, but it may cause aeromechanical instability due to the shift in the mass center. The other one is to design the overhang of the trailing edge flap. This will also be quite effective, but the design detail is beyond the scope of the present study, and will be addressed in future papers.

After mechanical tuning, which means that structural resonant frequency ω_m defined in Eq. (21) is tuned to the desired operating frequency, the actuation system is referred to as the *resonant actuation system*.

5.2 Electrical tailoring

In general, the frequency response (Eq. (19)) of the resonant actuation system with the shunt circuit will intersect that of the system without the shunt circuit at two invariant points [10,15]. The location of the intersection points depend on the inductance tuning δ defined in Eq. (21). When the magnitudes of these two points are equal, the inductance tuning, δ^*, for the series RL configuration is considered to be optimal:

$$\delta^* = \sqrt{1+\xi^2\eta^2} \tag{22}$$

Under the optimal inductance tuning, the aforementioned two invariant points are

$$\varpi_{1,2}^2 = 1+\xi^2\eta^2 \pm \frac{1}{2}\sqrt{2\xi^2\eta^2(1+\xi^2\eta^2)} \tag{23}$$

The frequency response for any given value of the resistance tuning, r, will pass through these two intersection points. An optimal value of r to produce the best (low magnitude) passive damping response, can be found by equating the magnitude of the frequency response [10,15], Eq. (19a), at $\varpi=\delta^*$ and that of the two invariant points,

$$r^* = \frac{\sqrt{2}\xi\eta}{1+\xi^2\eta^2} \tag{24}$$

These optimal tuning ratios δ^* and r^* will reduce the resonance peak, which is the main idea in many structural vibration control strategies. It has turned out that the voltage driving response can also be broadened at the resonance peak [15]. This scheme can be used to increase the bandwidth and robustness of the resonant actuation system. On the other hand, with such a design, the system will be fail-safe. That is, the system response will be bounded when active voltage/power fails.

With the aid of Eq. (23), the broadness of the resonance peak of the resonant actuation system, B_{ϖ}, can be defined by:

$$B_{\varpi} = |\varpi_1 - \varpi_2| \approx \frac{\xi\eta}{\sqrt{2}}\left(1+\frac{1}{16}\xi^2\eta^2\right) \tag{25}$$

where $\varpi_{1,2}$ are the two invariant frequencies after electrical tuning, which only depends on the generalized electro-mechanical coupling coefficient ξ and frequency ratio η between the electro-mechanical de-coupled and coupled systems.

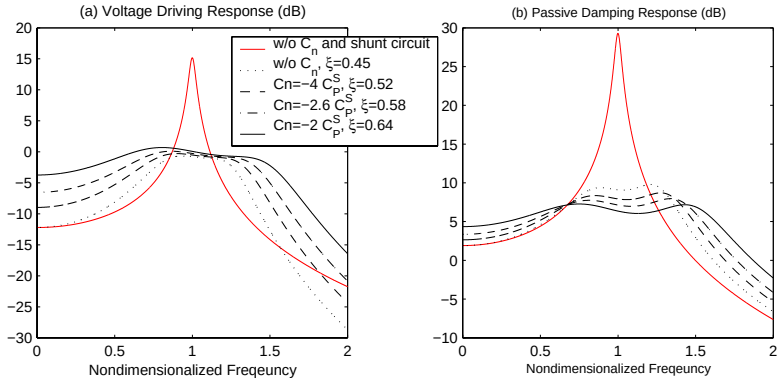

Figure 4: Frequency responses of the tube actuator under optimal resistance tuning for passive damping performance

The non-dimensionalized voltage driving and passive damping responses (Eq. (19)) versus frequency of the PZT tube actuator, under the optimal tuning ratios δ^* and r^* for passive damping performance, are presented in Fig. 4. The frequency responses are plotted with varying negative capacitance. As illustrated in Fig. 4(b), larger coupling coefficient of ξ will increase the shunt circuit passive damping performance. The passive damping responses of the resonant actuation system under the optimal tuning ratios for passive damping response, exhibit plateau shape around the structural resonant frequency. The optimal resistance-tuning ratio helps to make the plateau shape as flat as possible, while the voltage driving responses around the resonant frequency, Fig. 4(a), show distortions.

As far as the voltage driving responses are concerned, the optimal resistance-tuning ratio should be modified to flatten the plateau shape of the voltage driving frequency response around the resonant frequency. Making this plateau as flat as possible will provide active authority of constant magnitude around the operating frequency, which could be essential to compensate for uncertainties in the operating frequency. Following such guidelines, the optimal resistance-tuning ratio for the best voltage driving response, can be estimated by equating the non-dimensionalized transfer function, Eq. (19b), at two invariant points $\varpi_{1,2}$ to that at $\varpi=\delta^*$.

$$\bar{G}_{qV}\,|_{\varpi=\varpi_1} = \bar{G}_{qV}\,|_{\varpi=\delta^*} \tag{26}$$

Unlike the passive damping response case, it is difficult to find the closed form solution of the optimal resistance-tuning ratio, since the above equation is highly nonlinear. Thus, an iterative method is used to find the solution of Eq. (26). We will refer this resistance-tuning ratio as the *optimal resistance-tuning ratio* r_a^* for the *voltage driving performance*, which is designed to produce the best voltage driving response.

Table 3: Piezoelectric material properties of PZT-5H

Piezoelectric Constant	**Unit**	**BENDER**		**STACK**		**TUBE**	
Charge Constant	m/V or C/N ($\mathbf{10^{-12}}$)	d_{13}	**274**	d_{33}	**593**	d_{15}	**741**
Voltage Constant	V m/N ($\mathbf{10^{-3}}$)	g_{13}	**9.1**	g_{33}	**19.7**	g_{15}	**26.8**
Elastic Constant (Open Circuit)	N/m^2 ($\mathbf{10^{+10}}$)	C^D_{11}	**7.1**	C^D_{33}	**11.1**	C^D_{55}	**2.3**
Dielectric Constant	F/m ($\mathbf{10^{-8}}$)	ε^T_{33}	**3.011**	ε^T_{33}	**3.011**	ε^T_{11}	**2.765**
Piezoelectric Constant	V/m or N/C ($\mathbf{10^{+8}}$)	h_{13}	**6.461**	h_{33}	**21.867**	h_{15}	**6.164**
Impermittivity	m/F ($\mathbf{10^{+7}}$)	β^S_{33}	**8.217**	β^S_{33}	**8.217**	β^S_{11}	**5.856**

6 Numerical Results

In order to evaluate the trailing edge flap resonant actuation system, mach scaled helicopter rotor blade is considered as an example. The rotor has a blade diameter of 6 feet, a blade chord of 3 inches, and a nominal rotation of 2000 RPM. For comparison purposes, the non-dimensionalized frequency responses are evaluated and compared among actuators. Piezoelectric materials used in this study are PZT-5H piezoceramics for the bender, stack, and tube actuators (Table 3).

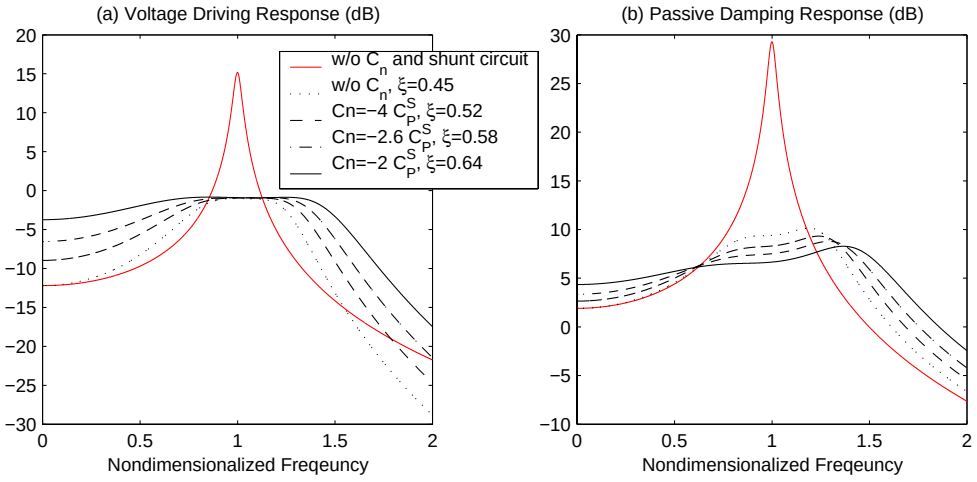

Figure 5: Frequency responses of the tube actuator under optimal resistance tuning for voltage driving performance

6.1 Non-dimensionalized frequency responses of the three actuator types

When appropriate amplification ratio and mechanical tuning frequency (usually, 3, 4 or 5 /rev of the main rotor speed) have been determined, the frequency responses between trailing edge flap deflection and control voltage or excitation force are evaluated, where the trailing edge flap deflection is calculated by Eq. (16). In the present study, the mechanical resonant tuning is achieved by adjusting the mass moment of inertia of the trailing edge flap.

The voltage driving and passive damping responses under optimal tuning ratios for passive damping performance for the PZT tube actuation system, calculated by Eqs. (23) and (25), are presented in Fig. 4. Results are obtained for the resonant actuation system that has a resonance at 4/rev of the main rotor speed. Under the optimal tuning ratio, r^*, not only the system passive damping ability is enhanced (lower vibration amplitude), the active authority is also improved (broader bandwidth) around the resonant frequency. The problem, however, is that the active authority around the resonant frequency shows a distorted (skewed) shape, which will cause inconsistency in its active action when the operating frequency varies due to system uncertainties.

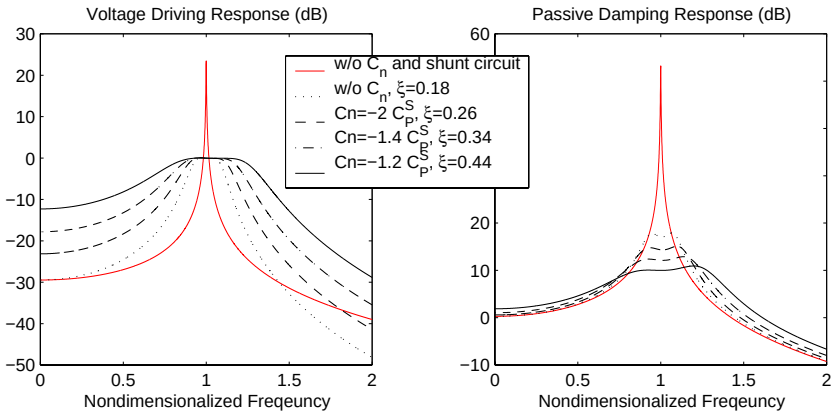

Figure 6: Frequency responses of the bender actuator under optimal resistance tuning for voltage driving performance

The voltage driving and passive damping responses of the PZT tube actuation system, under the newly introduced optimal resistance-tuning ratio for voltage driving performance (Eq. 27) are shown in Fig. 5, for various negative capacitance values. Now, we can see that the voltage driving responses, Fig. 5(a), around the resonant frequency are totally flat, while the passive damping responses, Fig. 6(b), show a distorted shape. With the negative capacitance, the bandwidth of the voltage driving response is increased. As shown in Fig. 5 and mentioned in Ref. 15, the active authority at the resonant frequency does not depend on the values of the negative capacitance.

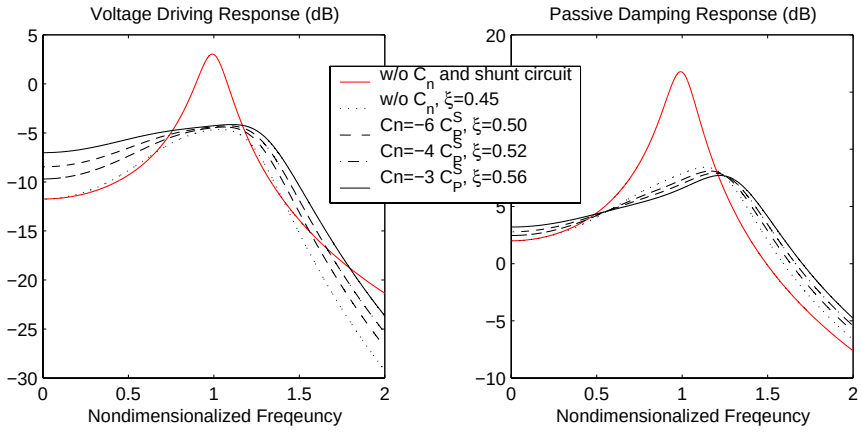

Figure 7: Frequency responses of the stack actuator under optimal resistance tuning for voltage driving performance

For bender and stack type actuators, the frequency responses under optimal resistance tuning for voltage driving performance are presented in Figs. 6 and 7. Once again, the voltage driving responses around the resonant frequency are nearly flat. Fig. 6 shows that the bender type actuator without the additional circuit has very large active authority around resonance but with very narrow bandwidth. Although the bandwidth can be increased with the circuitry design, it is still smaller than those of

the other types of actuation systems. On the other hand, the stack actuator has relatively large coupling coefficients compared to the bender and tube actuators. Thus, the voltage driving response around resonance of the stack actuation system without the circuit is much wider than the other actuation systems. In fact, for stack actuator, the effect of the negative capacitance is not as significant when compared to the other actuator types, as shown in Fig. 7. Notice that the presented results for all actuator types may be different when different amplification ratios and tuning mechanisms are used. This issue is beyond the scope of the present study and will be addressed in future papers.

Comparisons of non-dimensionalized quantities, such as the optimal resistance-tuning ratio for voltage driving performance, r_a^*, the generalized coupling coefficient, ξ, the ratio of the coupled and de-coupled system frequencies, η, and the broadness of the resonant peak, $B_\omega=|\varpi_1-\varpi_2|$, are shown in Table 4. As the negative capacitance value approaches the capacitance of PZT actuator, the plateau around the resonant frequency becomes much wider and the required optimal resistance is also increased. Cleary, with the negative capacitance C_n, the bandwidth B_ω, of the resonant actuation system is increased. As shown in Table 4, the non-dimensionalized quantities are also dependent upon the actuator type that determines which PZT material properties are used.

Table 4: Comparison of non-dimensionalized quantities among actuators

	C_n	r_a^*	ξ	η	$\lvert\varpi_1-\varpi_2\rvert$
Bender	without	0.234	0.181	1.017	0.130
	$-2.0C_P^S$	0.335	0.256	1.034	0.188
	$-1.4C_P^S$	0.448	0.338	1.063	0.256
	$-1.2C_P^S$	0.588	0.443	1.115	0.354
Stack	without	0.812	0.500	1.155	0.415
	$-6.0C_P^S$	0.885	0.548	1.195	0.472
	$-4.0C_P^S$	0.929	0.577	1.225	0.511
	$-3.0C_P^S$	0.977	0.612	1.265	0.562
Tube	without	0.620	0.452	1.121	0.363
	$-4.0C_P^S$	0.712	0.522	1.172	0.440
	$-2.6C_P^S$	0.778	0.576	1.223	0.509
	$-2.0C_P^S$	0.846	0.639	1.300	0.603

6.2 Mach-scaled PZT tube actuation system

In order to further evaluate the effectiveness of the proposed approach, two mach-scaled PZT tube actuation systems for trailing edge flap control are analyzed and compared. The trailing edge flap deflections are computed to quantify the active authority. For the purpose of comparison, a baseline actuation system is first defined based on the design presented in Ref. [9]: the length of the baseline PZT tube actuator is 4 inches, outer radius R_o is assumed to be 0.175 inches, the tube wall thickness is 0.1 inches, the flap length is 20% of rotor length, 7.2 inches, and the amplification ratio is 13. Note that the design principle of the baseline actuation system is to have its natural frequencies much higher than the operating frequencies (3, 4, 5/rev of the main rotor speed), which will provide a relative low but constant amplitude stroke within the operational bandwidth. To demonstrate the active authority improvement, a smaller 4/rev actuator is considered for the new resonant actuation system. The length of this smaller actuator is 2 inches, which is one-half of the baseline actuator, the trailing edge flap length is 2.4 inches (33% of the baseline), and the other dimensions are the same as the baseline.

In Fig. 8, the voltage driving and passive damping frequency responses are plotted, under the optimal resistance-tuning ratio for voltage driving performance. The vertical axis denotes the trailing edge flap deflections calculated by Eq. (16). The solid line indicates the voltage driving response of the baseline actuation system. The dotted and dash-dotted lines denote the voltage driving and passive damping responses, respectively, with both negative capacitor (-2.2 C_p^S) and shunt circuit. For the voltage driving responses, an electric field of 4 kV/cm is applied. For the passive damping response, the excitation force is assumed to be the same moment as that produced by the 4 kV/cm electric field. The resonant actuation system is tuned to the 4/rev (120 Hz) of the main rotor speed, by modifying the mass moment of inertia of trailing edge flap and amplification ratio.

Comparing the baseline and the new resonant actuation systems, we see that the active authority is significantly increased from 3 degree to 8 degree, as shown in Fig. 8. The flap deflections around the resonant frequency are almost constant (flat plateau) and the bandwidth reasonably large (approximately 80 Hz). The passive damping performance is also important for fail-safe reasons. As shown in Fig. 8, the proposed resonant actuation system can constrain the resonance peak under power loss or free flap situations, which makes the system fail-safe.

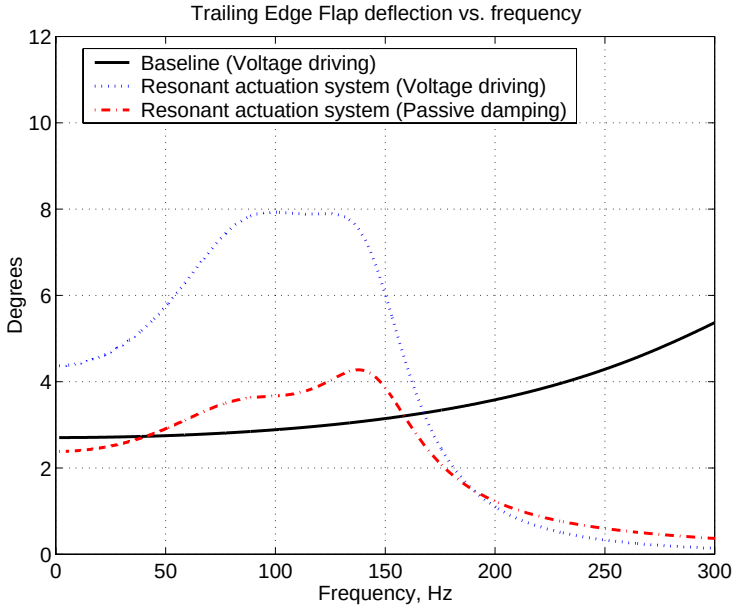

Figure 8: Trailing edge flap deflections for mach-scaled rotor

7 Conclusions

In this paper, a new approach is proposed to enhance the active authority of piezoelectric actuation systems, without the trade off between force and stroke. The idea is to first achieve a resonant driver through using mechanical tuning, and then increase the bandwidth and robustness of the resonant actuation system through electrical network tailoring. The new resonant actuation concept is evaluated on three types of actuators, namely the PZT bender, stack and tube. A coupled PZT actuator, trailing edge flap and electrical circuit dynamic model is derived. Utilizing the model, the required electrical circuitry parameters are determined. The inductance is first tuned such that the piezoelectric shunt frequency matches the mechanical resonant frequency. Negative capacitance is then used to broaden the actuation authority bandwidth around the operating frequency. To further enhance the robustness, an optimal resistance tuning ratio is derived such that the actuation authority frequency response near the resonant frequency can be flattened. The performances of the different actuation systems are analyzed and compared. To evaluate the proposed idea quantitatively, two mach scaled piezoelectric tube actuator-based trailing edge flaps for helicopter vibration control are used for comparison. It is demonstrated that the proposed resonant actuation system can indeed achieve both high active authority and robustness, as compared to a baseline system. The new flap device also has good fail-safe quality, due to the fact that the system is well damped. In other words, the flap response is well bounded with failure of the active source.

Acknowledgments

The authors acknowledge the support for this research work from the National Rotorcraft Technology Center, with technical monitor Dr. Yung Yu.

References

1. Chopra, I., "Status of Application of Smart Structures Technology to Rotorcraft Systems," *Journal of the American Helicopter Society*, Vol. 45, No. 4, Oct. 2000, pp. 228-252.

2. Milgram, J.H. and Chopra, I., "A Parametric Study for Actively Controlled Trailing Edge Flaps," *Journal of the American Helicopter Society*, Vol. 43, No. 2, April 1998, pp. 110-119.

3. Kim, J.-S., Smith, E.C., and Wang, K.W., "Active Load Control of an Articulated Composite Rotor Blade via Dual Trailing Edge Flaps," *44th AIAA Structures, Structural Dynamics, and Materials Conference*, Norfolk, Virginia, April 2003.

4. Koratkar, N.A. and Chopra, I, "Analysis and Testing of a Mach Scaled Helicopter Rotor with Piezoelectric Bender Actuated Trailing Edge Flaps," *SPIE's Smart Structures and Materials Symposium*, San Diego, March 1998.

5. Fulton, M.V. and Ormiston, R.A., "Hover Testing of a Small Scale Rotor with On-Blade Elevons," *Journal of the American Helicopter Society*, Vol. 46, No. 2, April 2001, pp. 96-106.

6. Clement, J.W., Brei, D., Moskalik, A.J., and Barrett, R., "Bench-Top Characterization of An Active Rotor Blade Flap System Incorporating C-Block Actuators," *39th AIAA Structures, Structural Dynamics, and Materials Conference*, Long Beach, April 1998.

7. Lee, T. and Chopra, I., "Design of Piezostack Driven Trailing Edge Flap Actuator for Helicopter Rotors," *Smart Materials and Structures*, Vol. 10, No. 1, Feb. 2001, pp. 15-24.

8. Prechtl, E.F and Hall, S.R., "An X-Frame Actuator Servoflap Actuation System for Rotor Control," *SPIE's Smart Structures and Materials Symposium*, San Diego, March 1998.

9. Centolanza, L.R., Smith, E.C., and Munsky, B., "Induced-Shear Piezoelectric Actuators For Rotor Blade Trailing Edge Flaps," *Smart Materials and Structures*, Vol. 11, Feb. 2002, pp. 24-35.

10. Hagood, N.W. and Von Flotow, A., "Damping of Structural Vibrations with Piezoelectric Materials and Passive Electrical Networks," *Journal of Sound and Vibration*, Vol. 146, No. 2, 1991, pp. 243-268.

11. Agnes, G.S., "Development of a Modal Model for Simultaneous Active and Passive Piezoelectric Vibration Suppression," *Journal of Intelligent Material Systems and Structures*, Vol. 6, No. 4, 1995, pp. 482-487.

12. Tsai, M.S. and Wang, K.W., "Control of a Ring Structure with Multiple Active-Passive Hybrid Piezoelectric Networks," *Smart Materials and Structures*, Vol. 5, No. 5, 1996, pp. 695-703.

13. Tsai, M.S. and Wang, K.W., "On the Structural Damping Characteristics of Active Piezoelectric Actuators with Passive Shunts," *Journal of Sound and Vibration*, Vol. 221(1), 1999, pp.1-22.

14. Behrens, S., Fleming, A.J., and Moheimani, S.O.R., "New Method for Multiple-Mode Shunt Damping of Structural Vibration using a Single Piezoelectric Transducer," *SPIE - The International Society for Optical Engineering*, 4331, 2001, pp. 239-250.

15. Tang, J. and Wang, K.W., "Active-Passive Hybrid Piezoelectric Networks for Vibration Control: Comparisons and Improvement," *Smart Structures and Materials*, Vol. 10, No. 4, August, 2001, pp. 794-806.

16. Standards Committee of the IEEE Ultrasonics, Ferroelctrics, and Frequency Control Society, 1987, An American National Standard: *IEEE Standard on Piezoelectricity*, The Institute of Electrical and Electronics Engineers, ANSI/IEEE Std 176-1987, New York.

17. Theodorson, T., "General Theory of Aerodynamic Instability and the Mechanism of Flutter," NACA Report No. 496, 1935.

18. Horowitz, P. and Hill, W., 1989, *The Art of Electronics*, Cambridge University Press.

19. Robert D. Blevins, 1979, *Formulas for Natural Frequency and Mode Shape*, Van Nostrand Reinhold Company